"Design, Synthesis & Characterization of Novel Electronic & Photonic BioMolecular Materials"

- **Michael J. Therien** (Chemistry/Penn):
  --novel non-biological co-factor design, synthesis & characterization for
  a) control of fast e^-- transfer over large distances &
  b) large molecular hyperpolarizabilities β

- **William F. DeGrado** (Biochemistry & Biophysics/Penn)
  --bio-inspired & computational peptide design for
  a) control of cofactor micro-environment
  b) control of assembly of peptide-cofactor complexes on macro-scale

- **Jeffrey G. Saven** (Chemistry/Penn)
  --"first-principles" *de novo* peptide design
  a) key to utilization of non-biological cofactors & non-biological amino acid analogues
  b) control of assembly of peptide-cofactor complexes on macro-scale

- **J. Kent Blasie** (Chemistry/Penn)
  --structural characterization of non-crystalline materials
  a) key to translation of microscopic molecular property into a macroscopic materials property

Artificial Protein Design: Maquettes

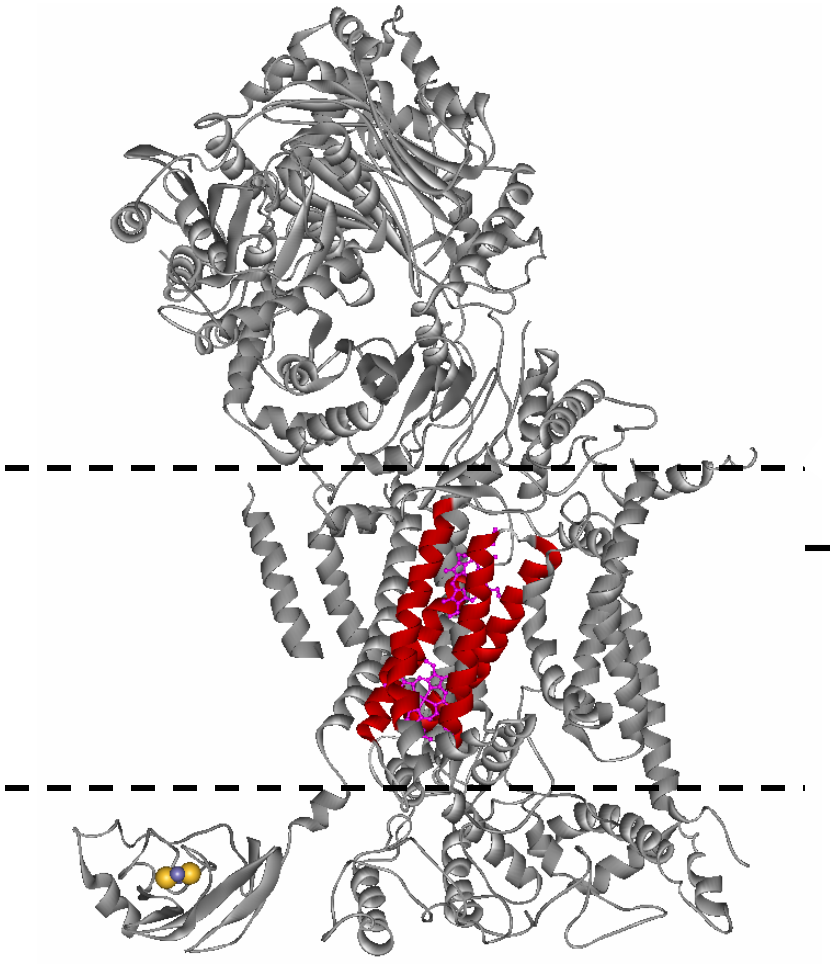

Cytochrome *bc1* complex

"de novo"
Design via
Bioinspiration

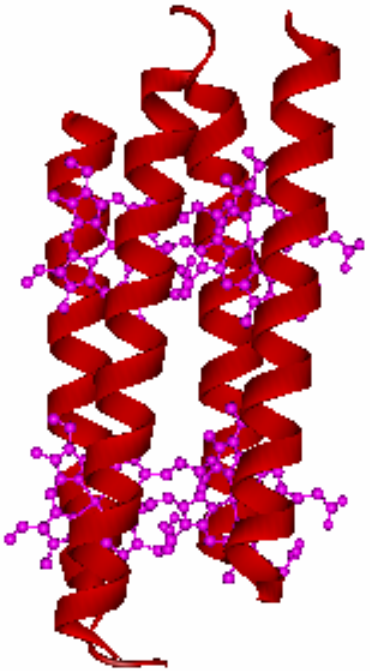

H10H24 (water soluble)

Robertson *et al.* **Nature** 368, pp. 425-432 (1994)

Maquette-Based BioMolecular Materials

Functional Maquette Peptides

Assemble on Macroscopic Scale

Collective Behavior

New BioMolecular Materials

Novel Peptide Amphiphile Design

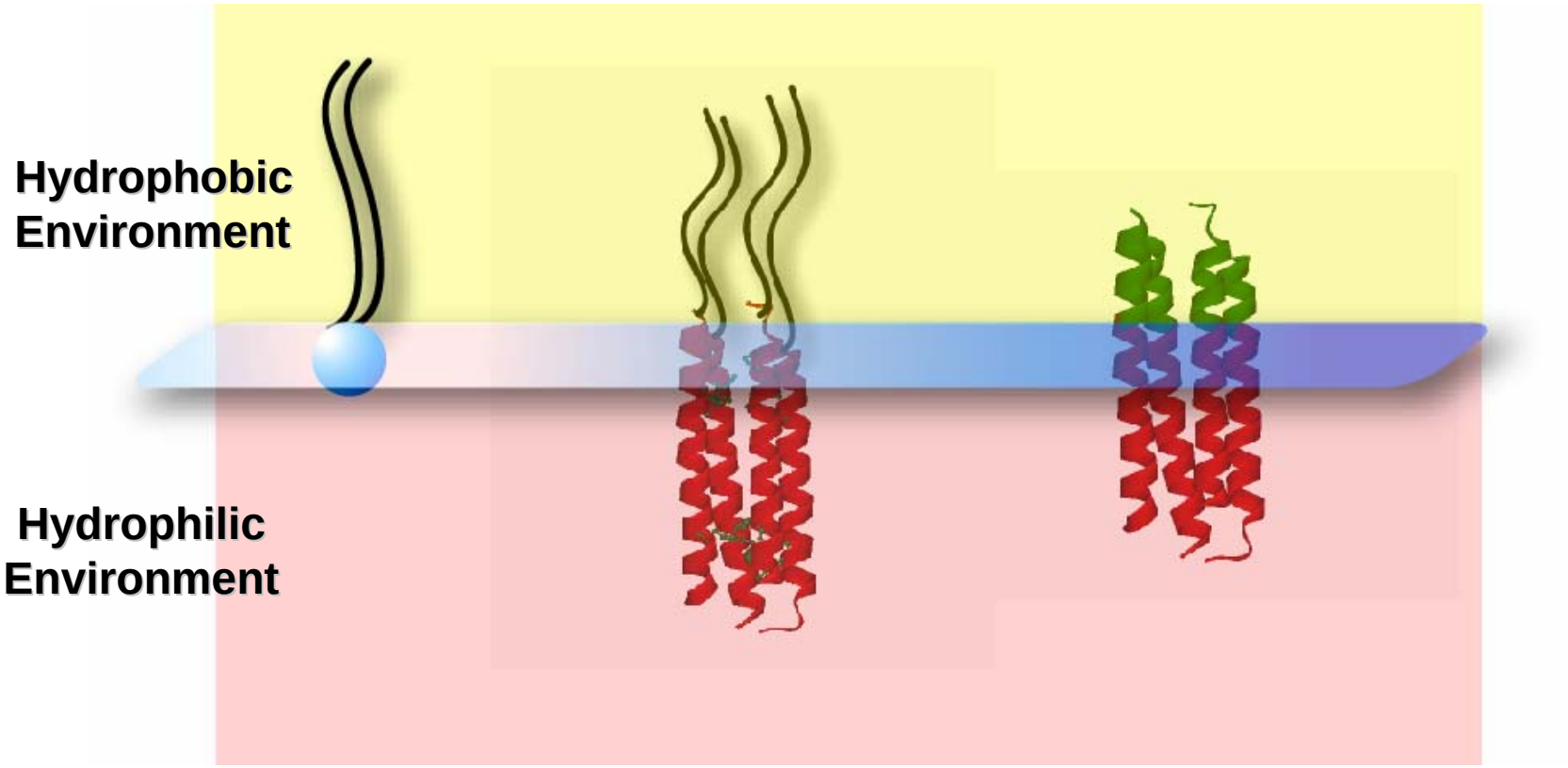

Phospholipid

BBC16 Maquette

Membrane Protein Maquette

Vectorial Orientation

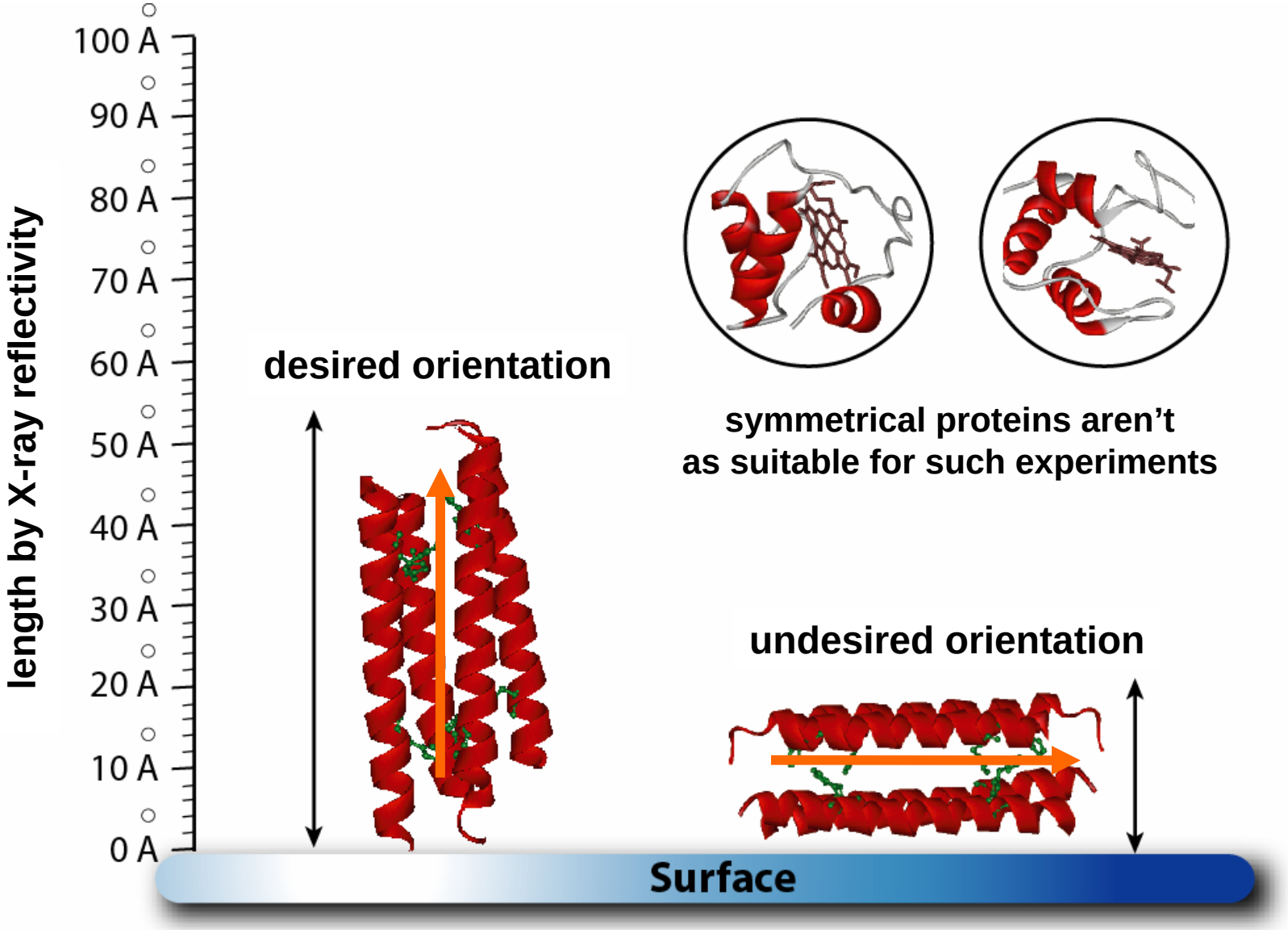

AP Family of Maquettes

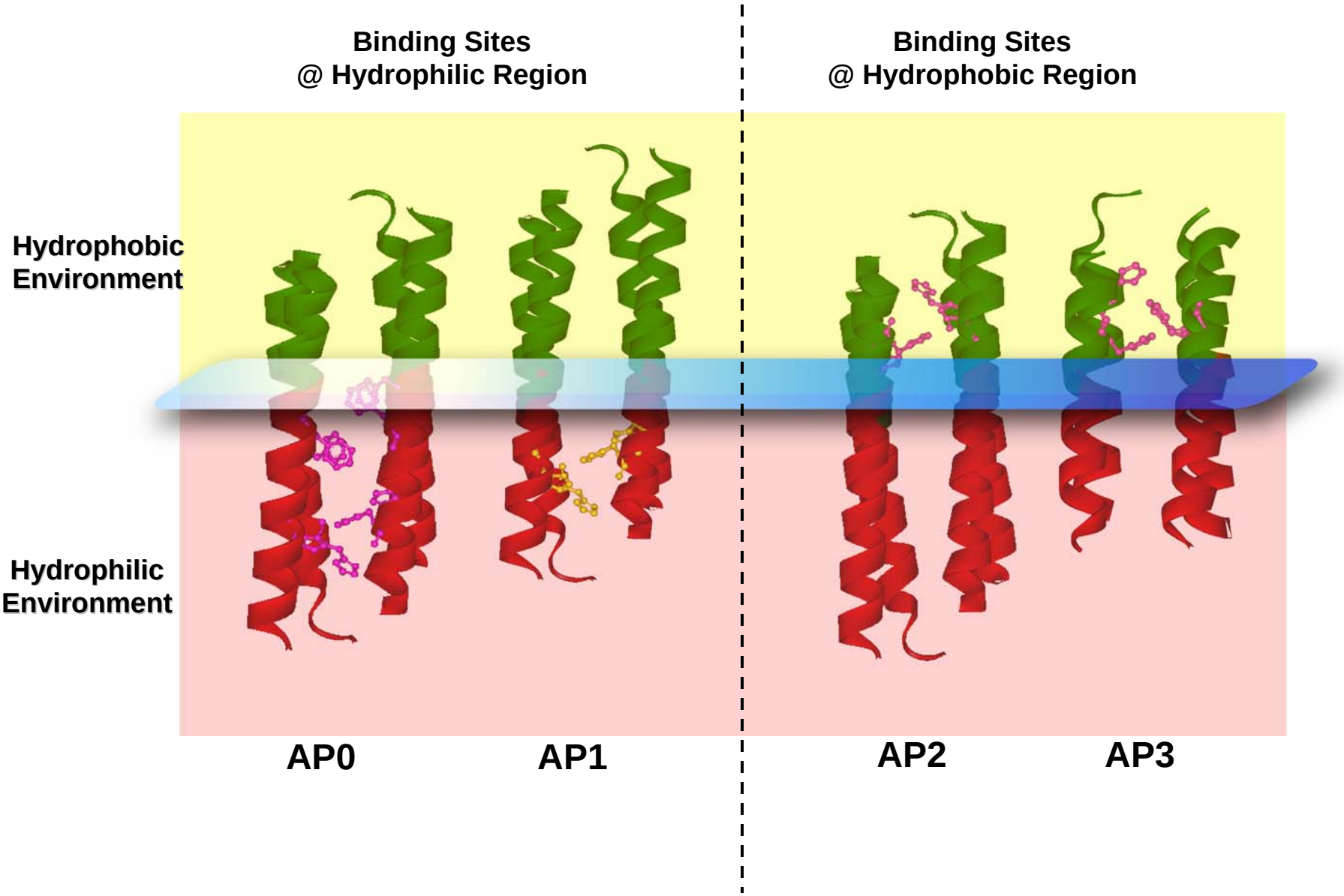

AP Family Peptides

AP0

Ac-EIWKLHEEFLKKFEELLKLHEERLKKLLLLALLQLLLALLQLGGC-$CONH_2$

BB

Inspired by LS_2

AP1

Ac-SSDPLVVAASIIGILHFILWILDRGGNGEIFKQHEEALKKFE-$CONH_2$

TM of M2 (influenza virus)

Partial HP-1

AP2

Ac-IIMAIAMVHLLFFFEIWKEFEEALKKFEEALKEFEELKKL-$CONH_2$

Partial D helix cyt. bc_1

HP-1

AP3

Ac-CGGGIIMAIAMVHLLFLFEIWKQFEEALKKFE-$CONH_2$

Partial D helix cyt. bc_1

Partial HP-1

AP0 Kd Binding

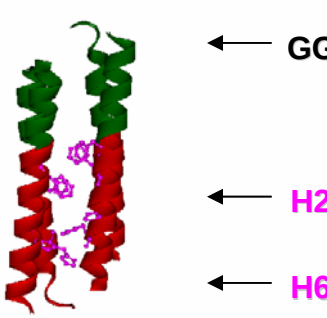

- **AP0 (H6A20) bundle binds 2 hemes/bundle**
- **K_{d1} = 60 nM**
- **K_{d2} = 700 nM**

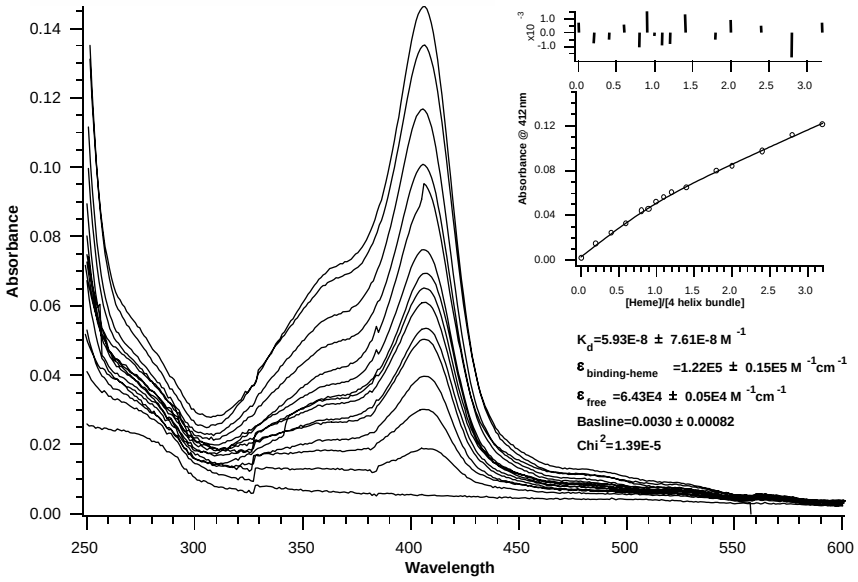

Buffer Condition: 50mM KPi, 0.9% ß-OG, pH=8.0, 25°C
Peptide Concentration: BA2 (H10A24)dimer, 0.5 um (4 helix-bundle)
Data File Directory: shixin/experiment/data/hemetitration/H10A24_0305_spec2.pxp

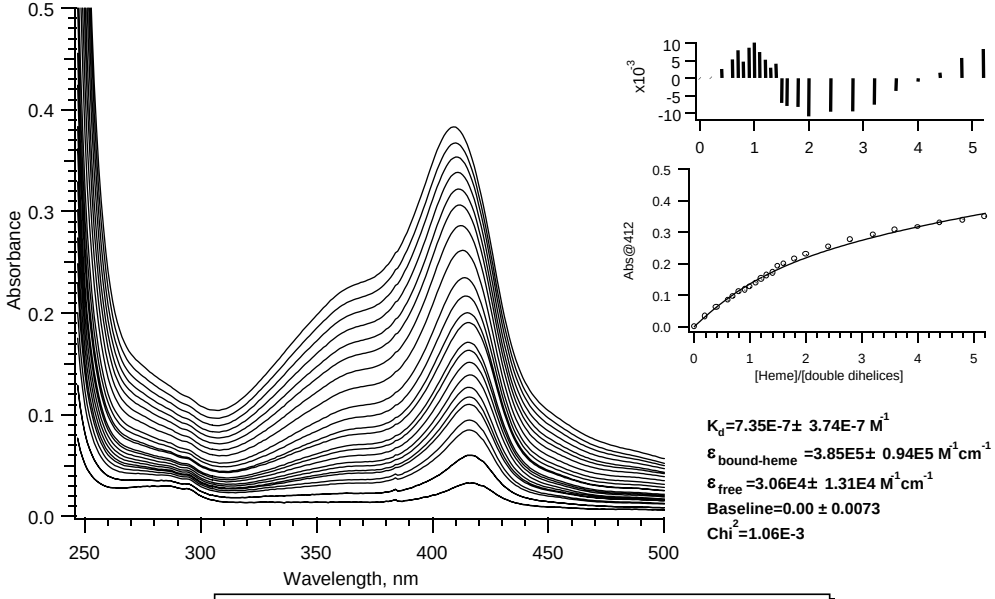

Buffer Condition: 50mM KPi, 0.9% ß-OG, pH=8.0, 25°C
Peptide Concentration: BA2(H10A24) 0.8 um (4 helix-bundle)
Data File Directory: shixin/experiment/data/heme_tritration/H10A24dim_0517_spec.pxp

AP0 Kd Binding

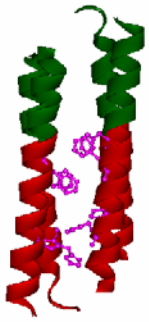

- **AP0 (H6A20) bundle binds 2 hemes/bundle**
- **K_{d1} = 60 nM**
- **K_{d2} = 700 nM**

First Heme

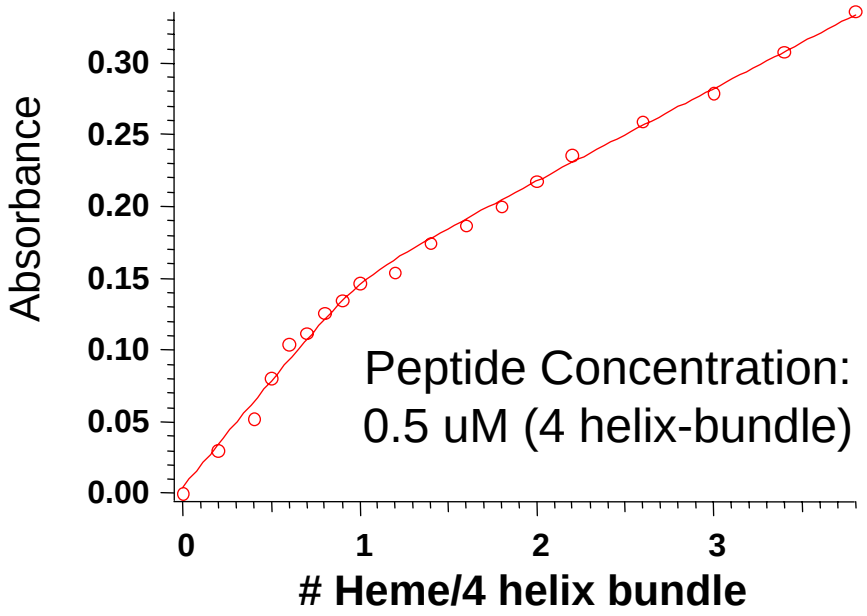

Second Heme

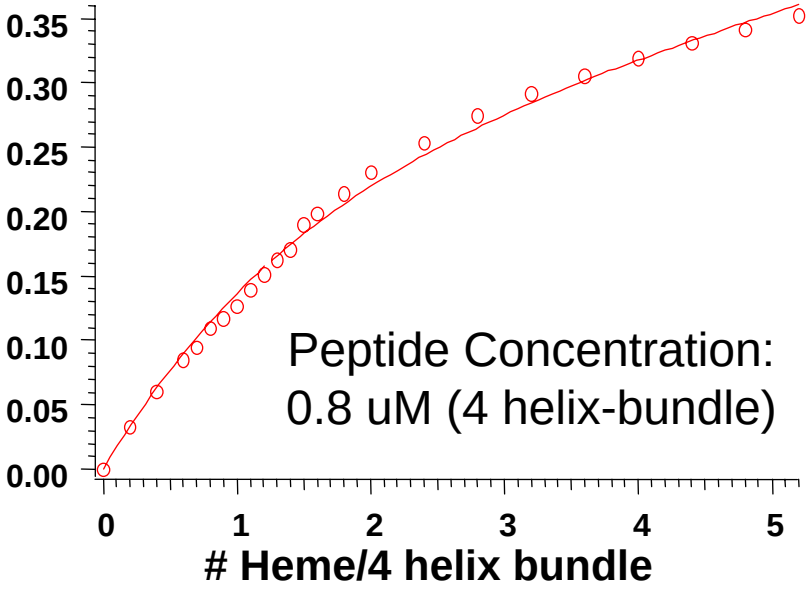

AP2 Kd Binding

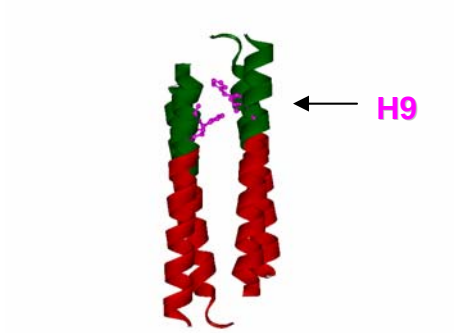

- **AP2 bundle binds 2 hemes/bundle**
- **K_{d1} = 40 nM**
- **K_{d2} = 3 uM**

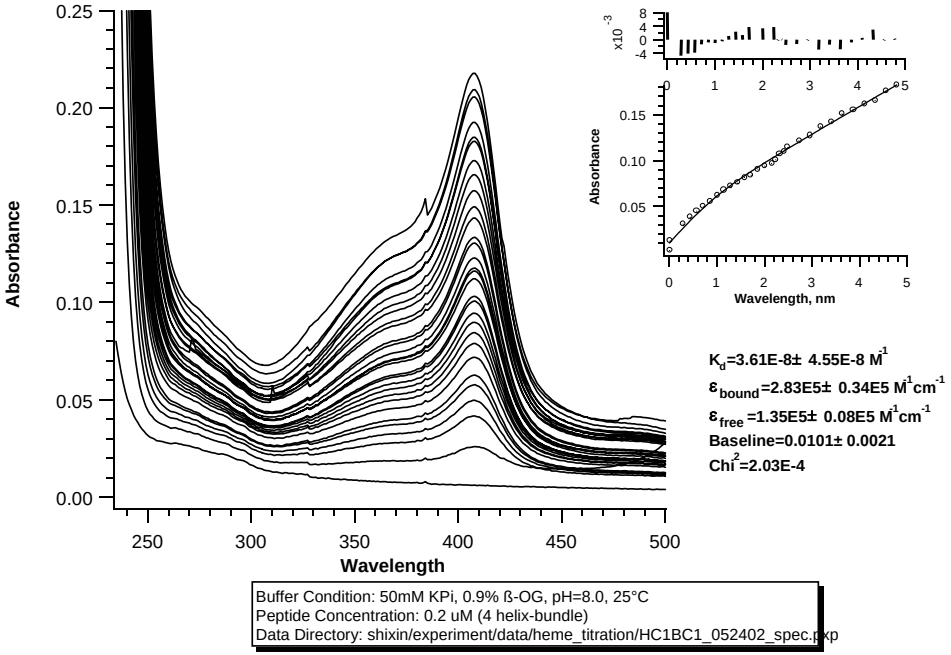

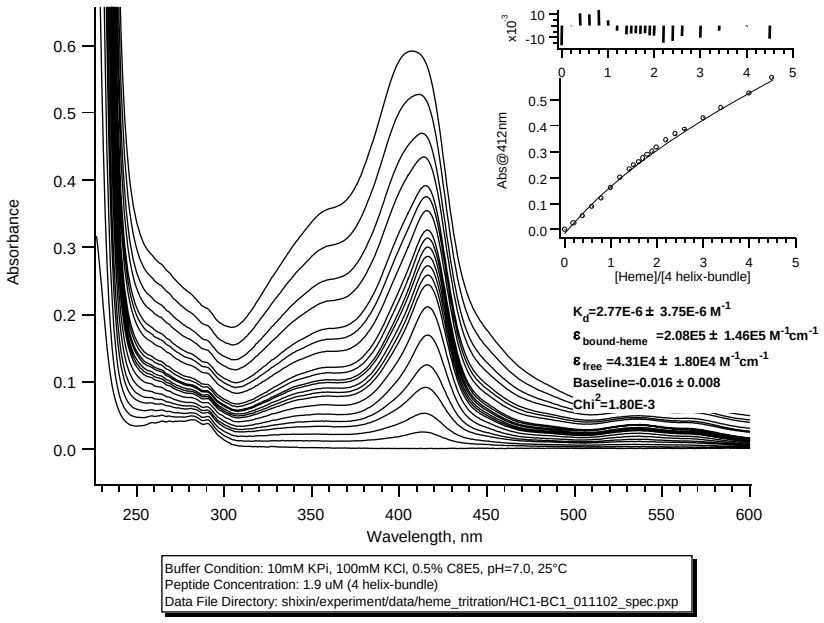

AP2 Kd Binding

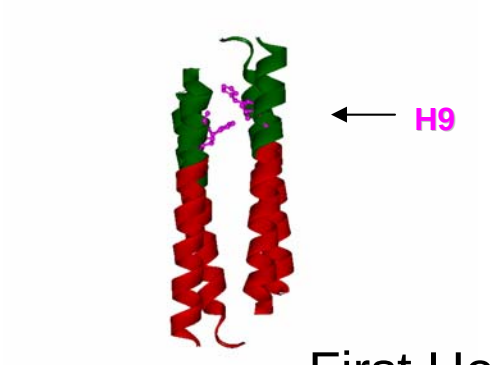

- **AP2 bundle binds 2 hemes/bundle**
- **K_{d1} = 40 nM**
- **K_{d2} = 3 uM**

First Heme

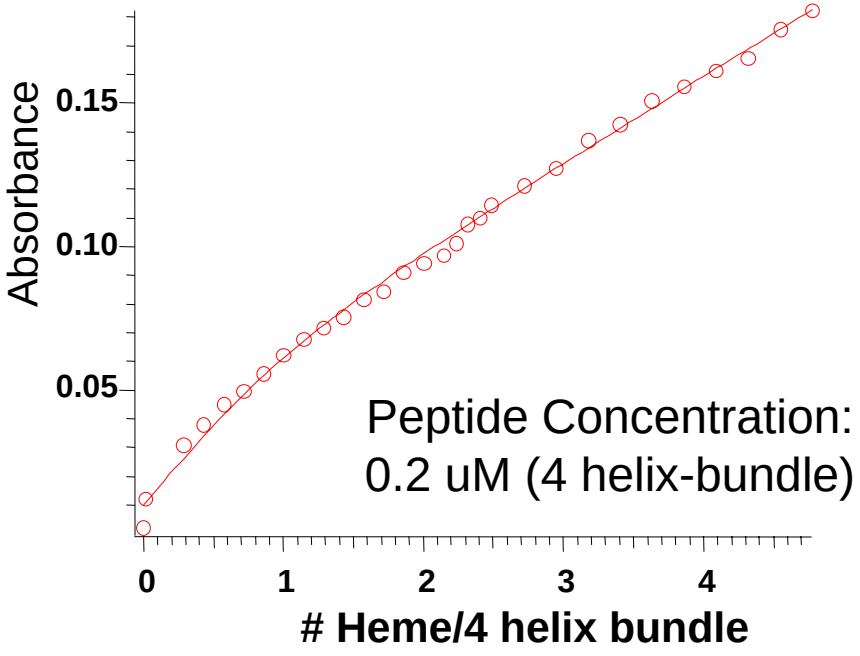

Second Heme

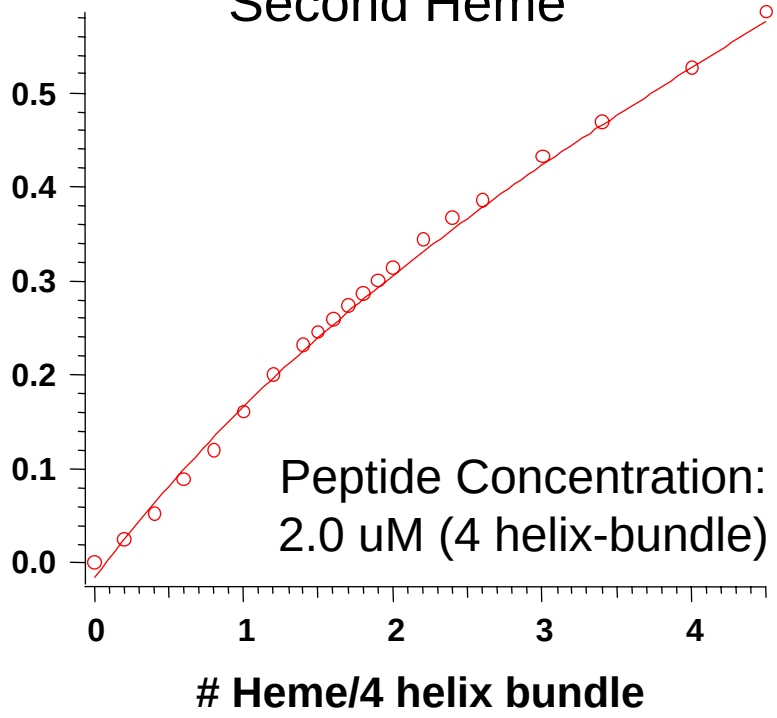

AP2 Binds Bacteriochlorophylls

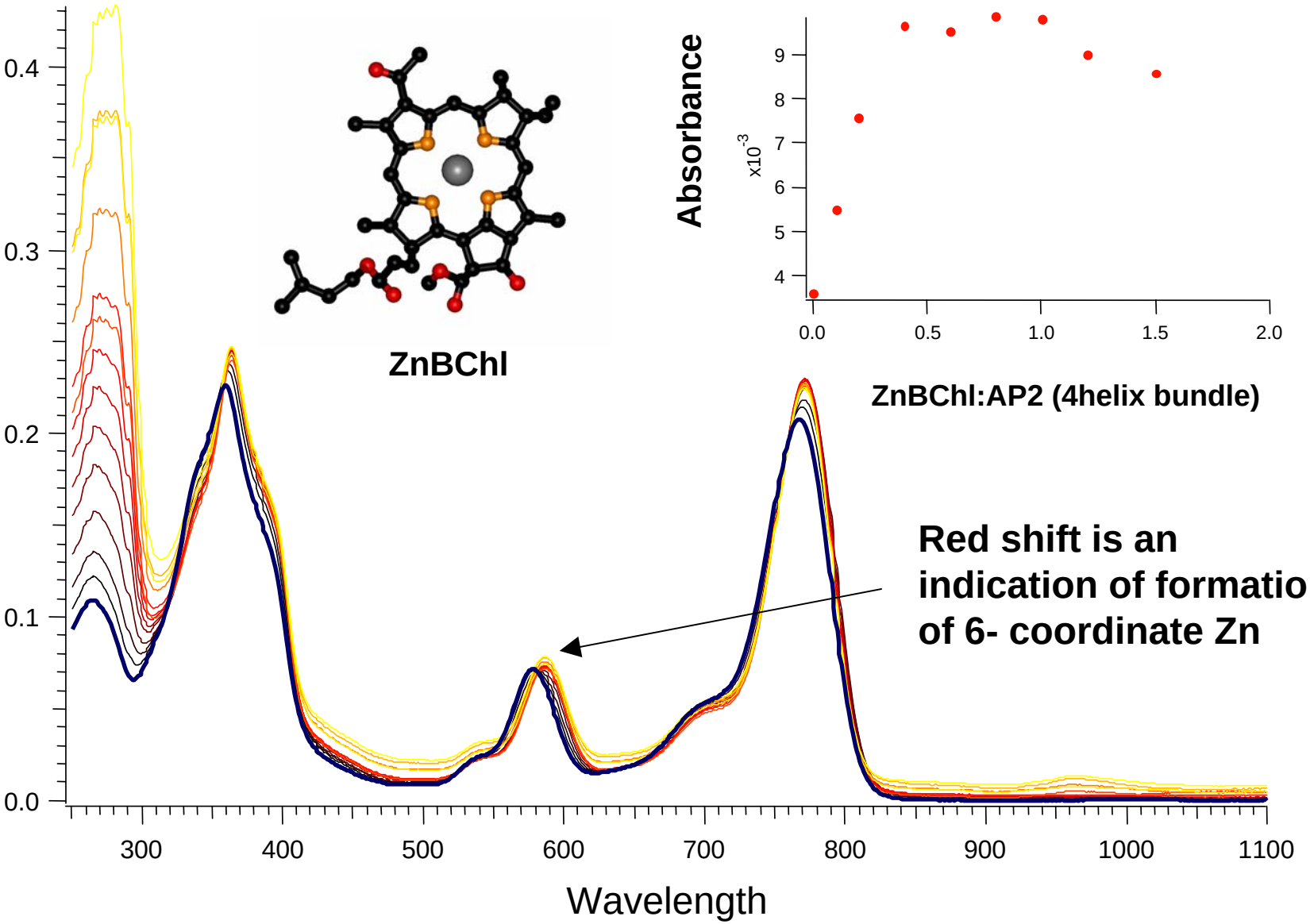

Structure of non-biological cofactors for electron transfer & non-linear optics applications: donor-bridge-acceptor "push-pull" extended π-electron systems

(sub-picosecond e^--transfer & large molecular hyperpolarizabilities β)

Zn-3-3-Zn

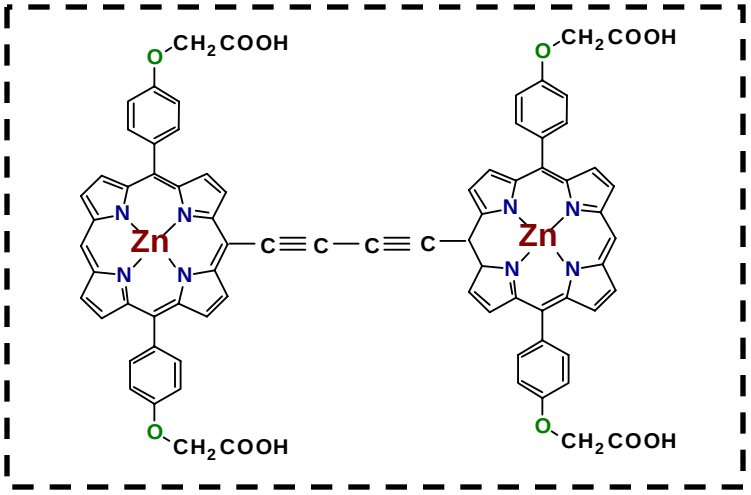

Ru-Zn

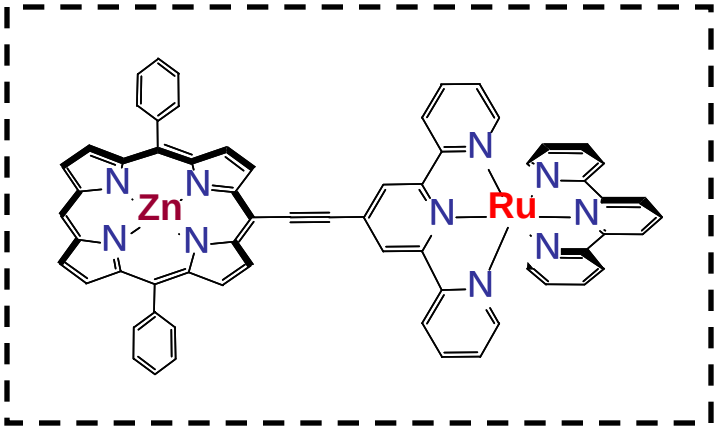

AP0

AP2/AP3

Zn-3-3-Zn
H6F20

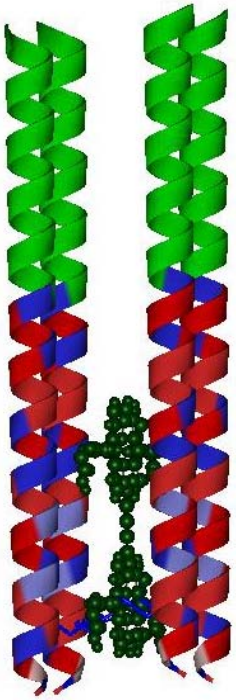

Zn-3-3-Zn
F6H20

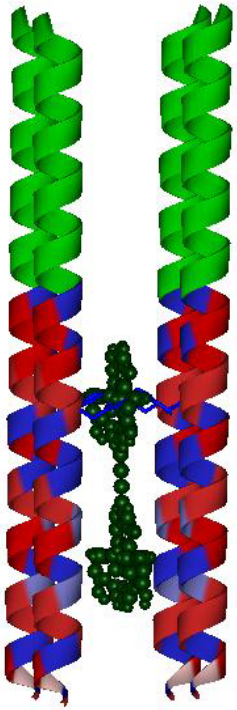

Zn-3-3-Zn
F6H20

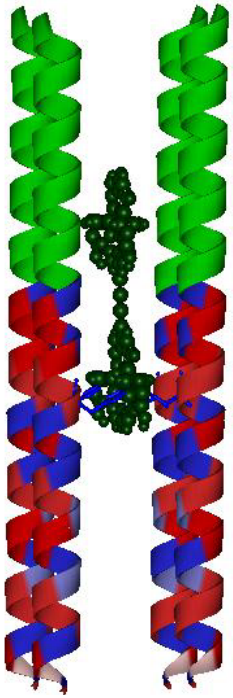

Zn-3-3-Zn
H9

QuickTime?and a
TIFF (LZW) decompressor
are needed to see this picture.

Electronic spectra: binding of non-biological cofactors in core of *hydrophilic* domain of amphiphilic 4-helix bundle AP0 via axial histidyl coordination

AP0/Zn33Zn

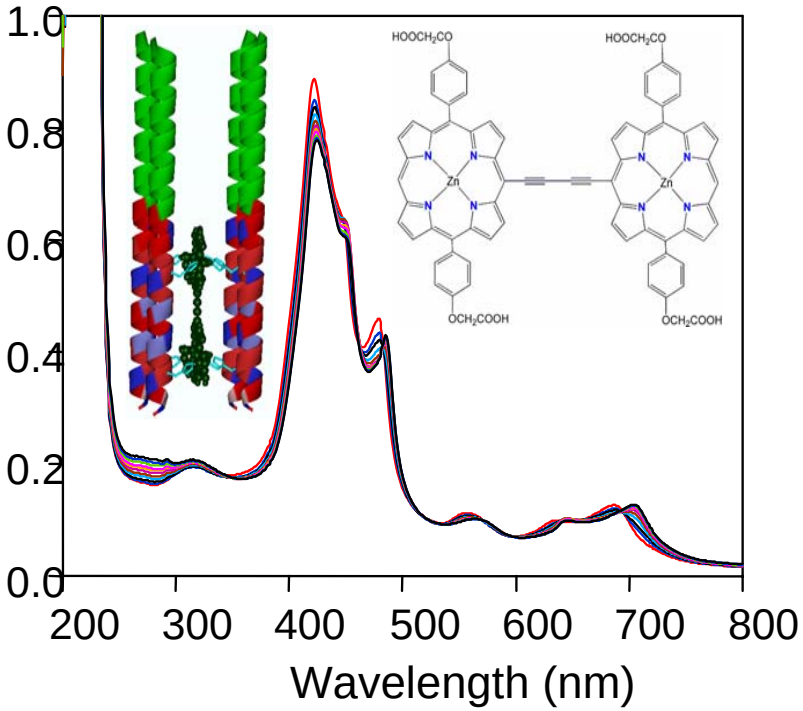

AP0/Zn-Ru

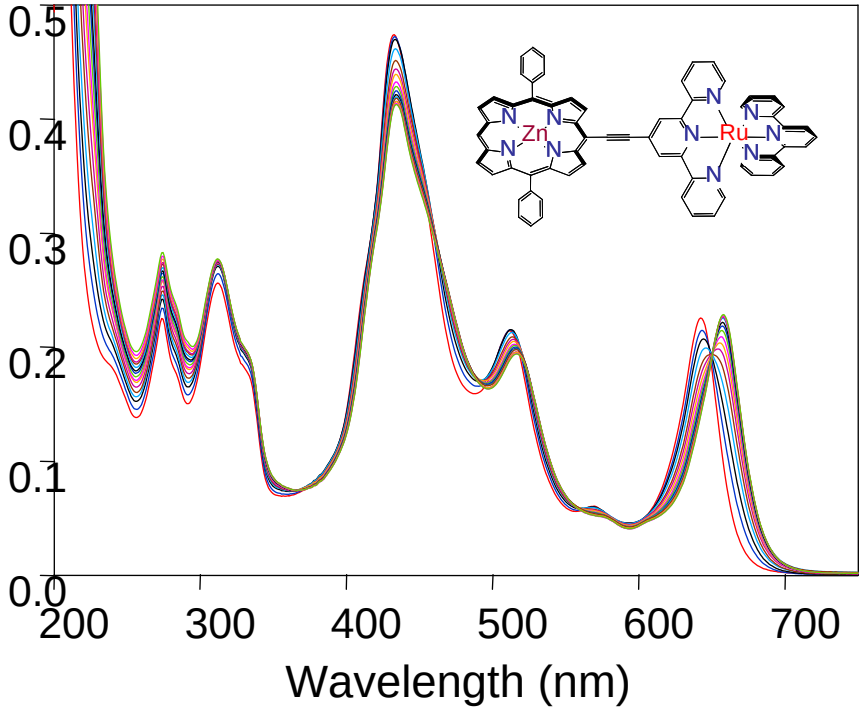

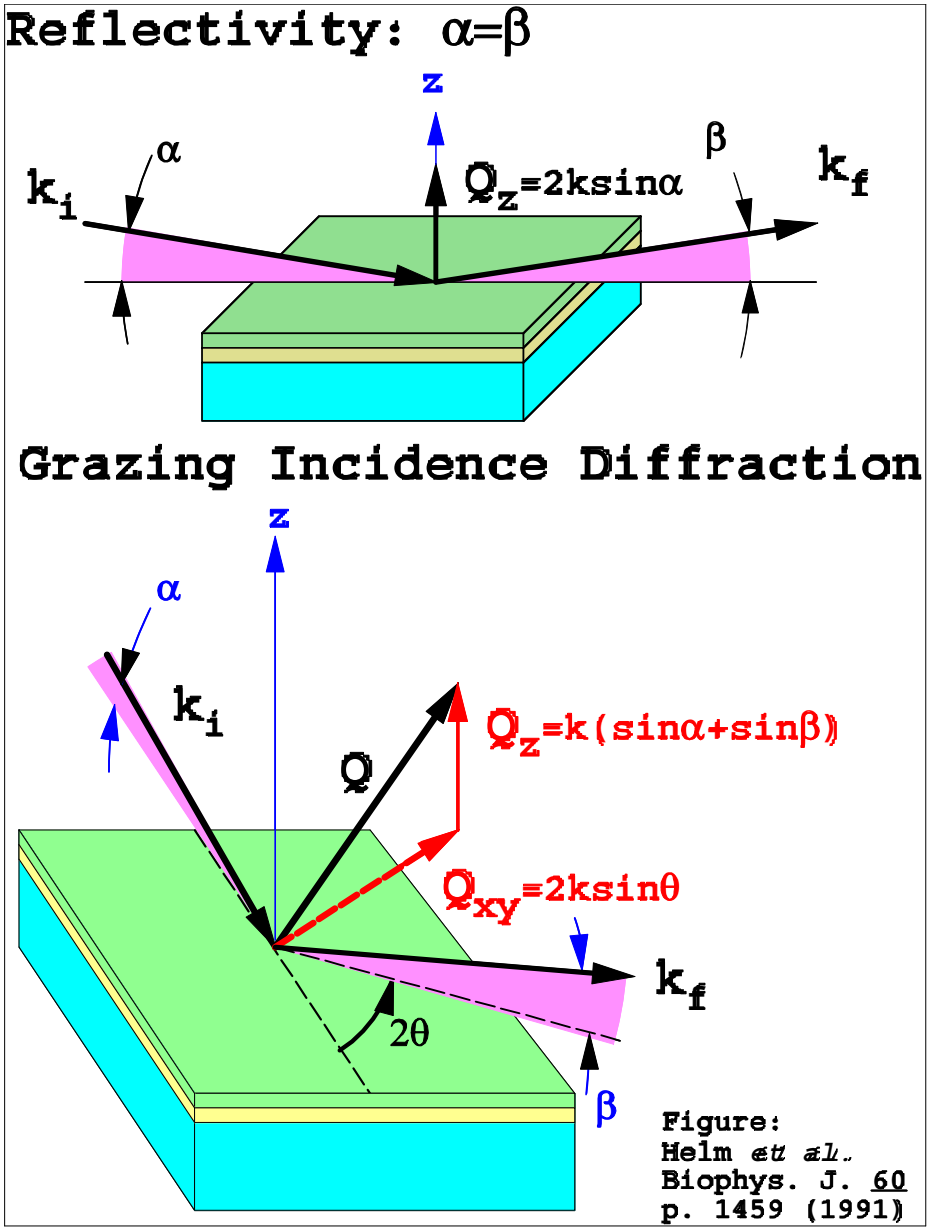

Figure:
Helm *et al.*
Biophys. J. 60
p. 1459 (1991)

PHYSICAL REVIEW B **67**, 224201 (2003)

Solution to the phase problem for specular x-ray or neutron reflectivity from thin films on liquid surfaces

J. Kent Blasie, Songyan Zheng, and Joseph Strzalka
Department of Chemistry, University of Pennsylvania, Philadelphia, Pennsylvania 19104-6323
(Received 25 February 2003; published 5 June 2003)

The phase problem for specular x-ray and neutron reflectivity from liquid surfaces and thin films on liquid surfaces can be solved in the distorted-wave Born approximation. The gradient of the scattering-length density (SLD) profile normal to the plane of the surface is bounded in these cases. This provides a powerful constraint allowing the phase problem to be solved with no *a priori* assumptions via an iterative Fourier refinement procedure applied to the Fresnel-normalized reflectivity. The critical boundary condition can be determined experimentally from the autocorrelation of the gradient profile obtained via an inverse Fourier transform of the Fresnel-normalized reflectivity without phase information. The phase solution and the resulting gradient SLD profile can be shown to be unique, and therefore unambiguously determined, when all of phase space is systematically explored for particular cases, especially for thin films on liquid surfaces. This gradient SLD profile can then be integrated either numerically, or better, analytically to provide the scattering-length density profile itself on an absolute scale.

DOI: 10.1103/PhysRevB.67.224201 PACS number(s): 68.18.Fg

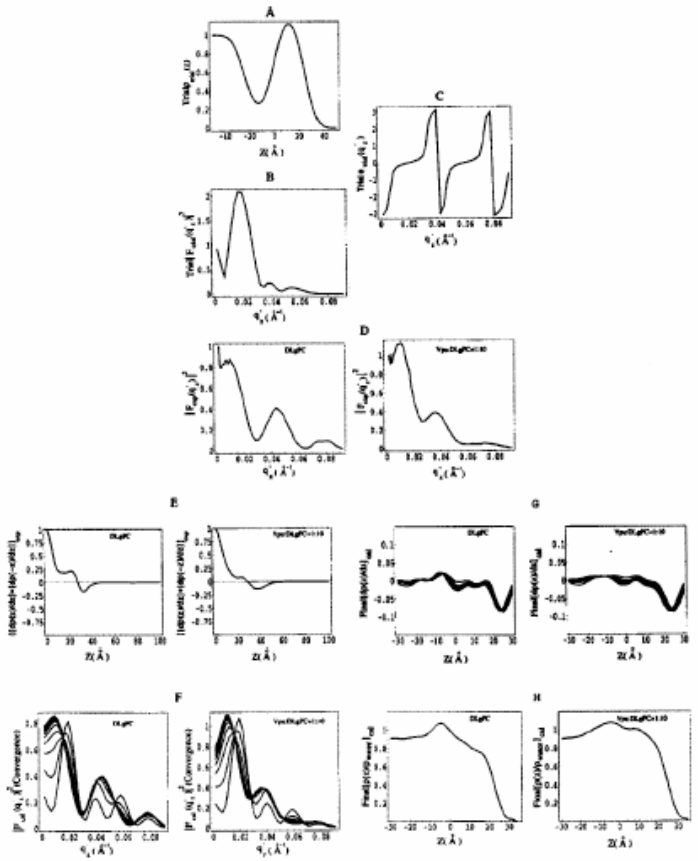

FIG. 1. Illustration of the box-refinement method of analysis for Fresnel-normalized x-ray reflectivity data from Langmuir monolayers of the pure diacylphospholipid DLgPC and its binary mixture with an HIV-1 accessory protein Vpu at a DLgPC/Vpu mole ratio of 10:1. In this and subsequent figures, reciprocal space functions are plotted vs q_z' (Å^{-1}) as defined in the distorted-wave Born approximation (see text), but where $|q_z| = (2 \sin\theta)/\lambda$ instead of $|q_z| = (4\pi \sin\theta)/\lambda$; all real space functions are plotted vs the profile coordinate z(Å). (A) Trial electron density profile $\rho_{trial}(z)$ used to initiate the box refinement. (B) Modulus squared $|F_{trial}(q_z')|^2$ of the Fourier transform of the gradient $[d\rho_{trial}(z)/dz]$ as a function of photon momentum transfer q_z'. (C) Phase $\phi_{trial}(q_z')$ of the Fourier transform of the gradient $[d\rho_{trial}(z)/dz]$ as a function of photon momentum transfer q_z'. Only this trial phase function originating from the trial electron density profile $\rho_{trial}(z)$ is used to initiate the box refinement. (D) Experimental normalized reflectivity $R(q_z')/R_F(q_z')$ expressed as a function of photon momentum transfer q_z', $|F_{trial}(q_z')|^2$. Note that neither case agrees with the modulus squared $|F_{trial}(q_z')|^2$ of the Fourier transform of the gradient $[d\rho_{trial}(z)/dz]$ shown in (B). (E) Inverse Fourier transform of the experimental $|F_{expt}(q_z')|^2$ which provides the autocorrelation of the gradient of the electron density profile $\{[d\rho_{expt}(z)/dz] \otimes [d\rho_{expt}(-z)/dz]\}$ for the monolayer. The box constraint, key input to the box refinement analysis, was chosen to be $L = 60$ Å, well beyond the last significant feature at $z \approx 40$ Å. (F) The convergence of the calculated $|F(q_z')|^2$ from the box-refinement to the experimental $|F_{expt}(q_z')|^2$ for iterations 1–10, 20, 30, 40, 50. (G) The convergence of the calculated $d\rho(z)/dz$ from the box refinement to the final $d\rho_{expt}(z)/dz$ for iterations 1–10, 20, 30, 40, 50. (H) The numerical integration of the final converged $d\rho(z)/dz$ to the absolute electron density profile for the monolayer $\rho_{expt}(z)$ itself. (This figure reprinted from Ref. 4 with permission of the Biophysical Society.)

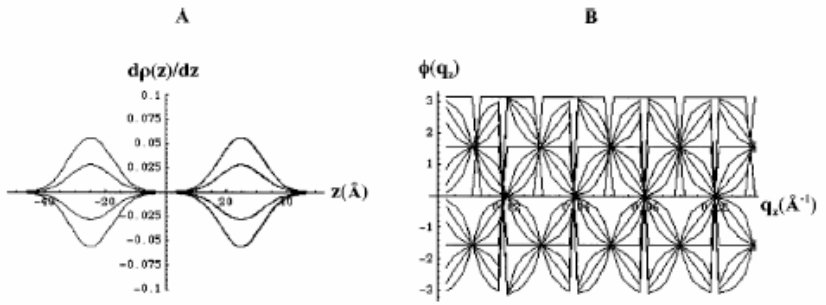

FIG. 2. The q_z-region of phase space accessed in the Fresnel-normalized x-ray reflectivity data shown in Fig. 1 was systematically explored using a finite set of gradient electron density profiles $d\rho(z)/dz$. These were based on all possible combinations of two Gaussian functions, each of five possible amplitudes (e.g., 0, $\pm\Delta$, $\pm 2\Delta$), and separated by 50 Å, the maximum extent of the bounded region in which the experimental gradient profiles are nonzero, thereby providing gradient profiles ranging from totally symmetric (even) to totally antisymmetric (odd) with intermediate asymmetric cases, as shown superimposed in (A). A superposition of the phase functions $\phi(q_z)$ of the Fourier transforms $F(q_z')$ of this set of gradient profiles, shown in (B), demonstrating their adequacy in searching the available phase space over this range of momentum transfer q_z accessed.

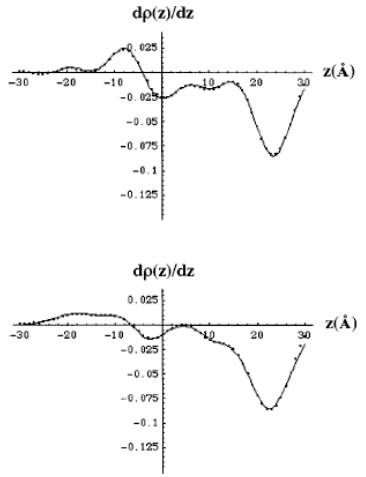

FIG. 4. Gradients of the monolayer electron density profiles $d\rho(z)/dz$ derived unambiguously from the experimental Fresnel-normalized x-ray reflectivity data via the box-refinement method, exactly as in Ref. 4, are shown as the dotted lines for the pure phospholipid DLgPC (top) and its binary mixture with an HIV-1 accessory protein Vpu at a DLgPC/Vpu mole ratio of 10:1 (bottom). The minimum representing the hydrocarbon/helium interface occurs in the region $+20$ Å$< z < +26$ Å in both monolayer profiles as shown here, which places that for the polar headgroup/hydrocarbon chain interface at the $z = 0$ Å origin for the pure DLgPC case, that choice being entirely arbitrary and of no other consequence. The best nonlinear least-squares fits of the sum of five Gaussian functions to the gradients of the monolayer electron density profiles $d\rho(z)/dz$ from box refinement are shown as the solid lines.

Electron Density Profiles for apo- *vs.* holo-AP2 for FePPIX (heme)

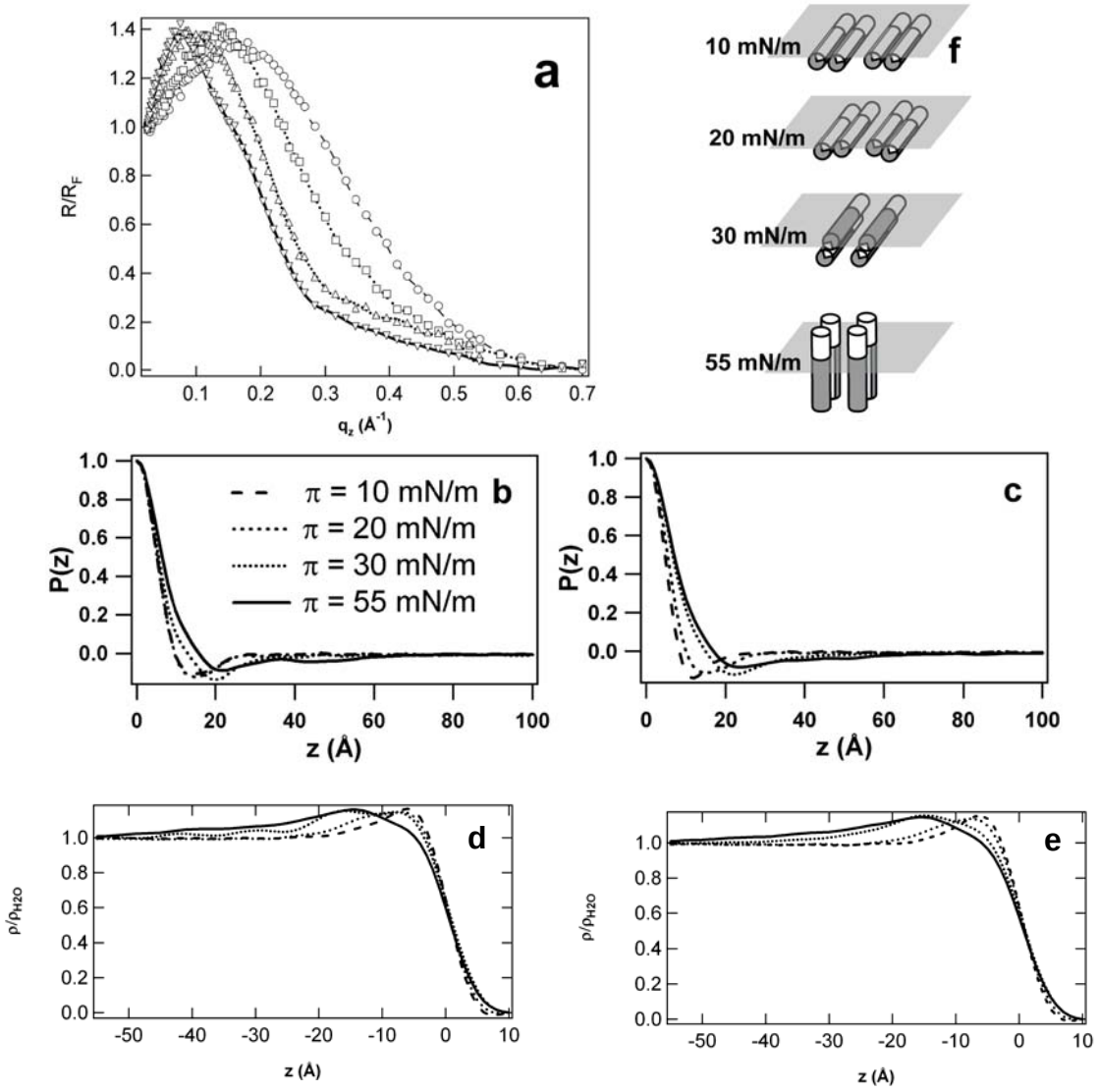

Molecular Dynamics (Theory)

Effect of Cofactor Incorporation for F6H20 AP0 & FePPIX

apo-AP0 peptide

holo-AP0:FePPIX peptide

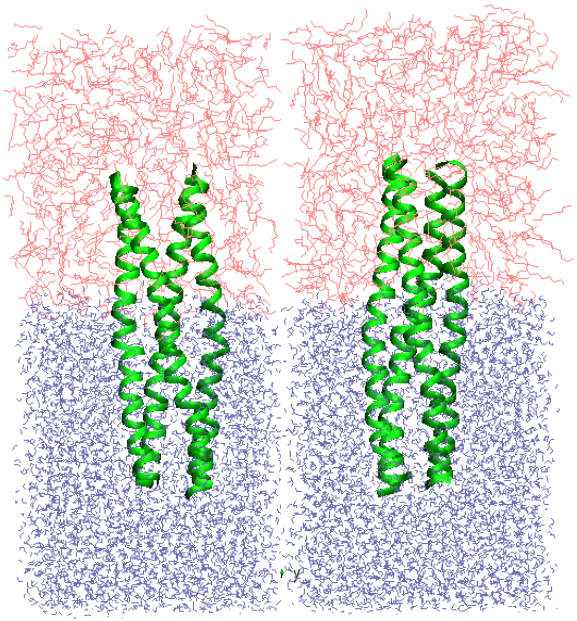

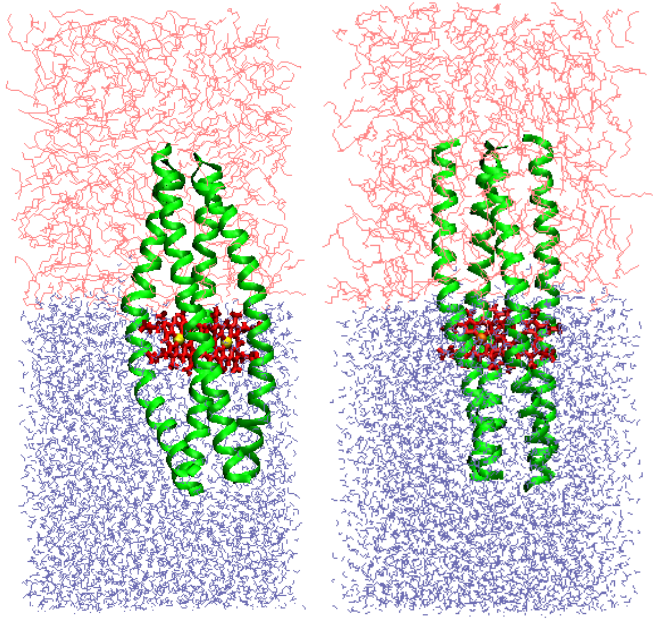

$\left\langle \left| F(Qxy, Qz) \right|^2 \right\rangle_t$

$\left\langle \left| F(Qxy, Qz) \right|^2 \right\rangle_t$

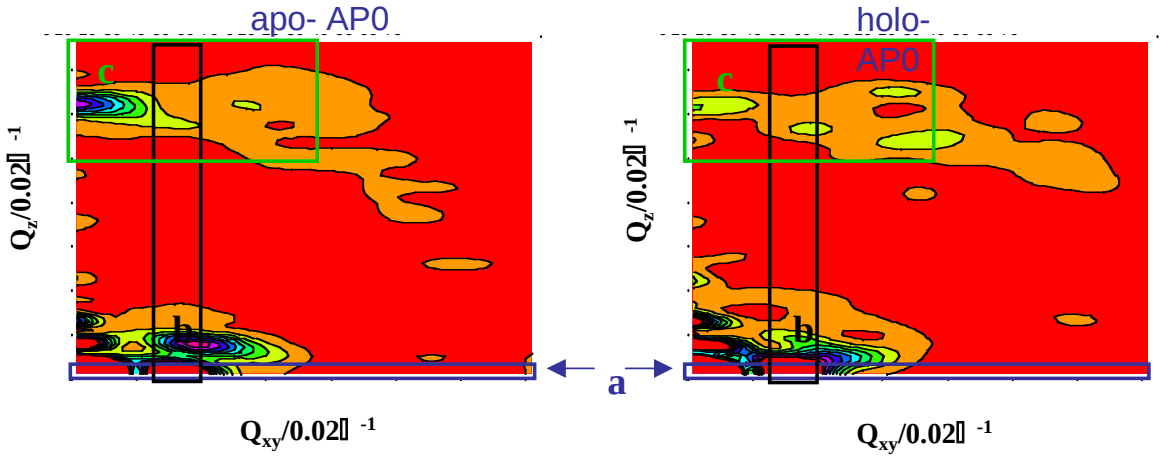

Electron Density Profiles for apo- & holo-AP0 and Zn-3-3-Zn

Profiles: Apo-AP0

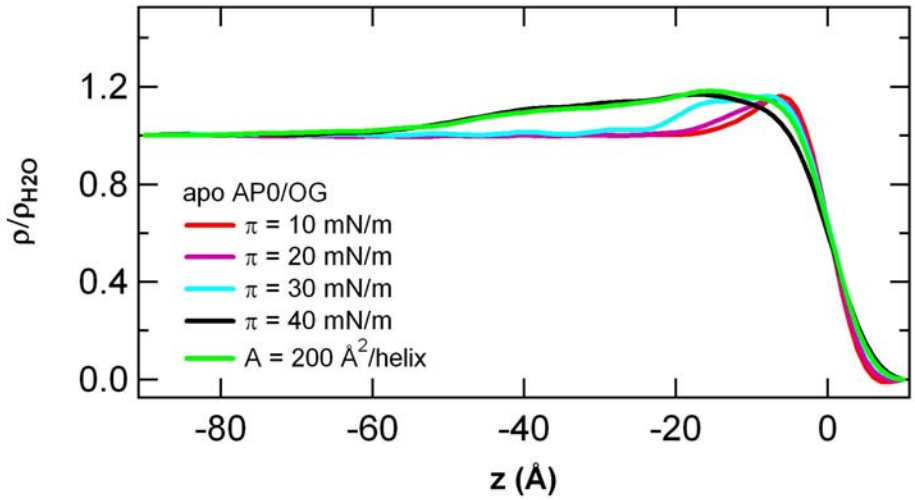

Profiles: Holo-AP0 Zn-3-3-Zn

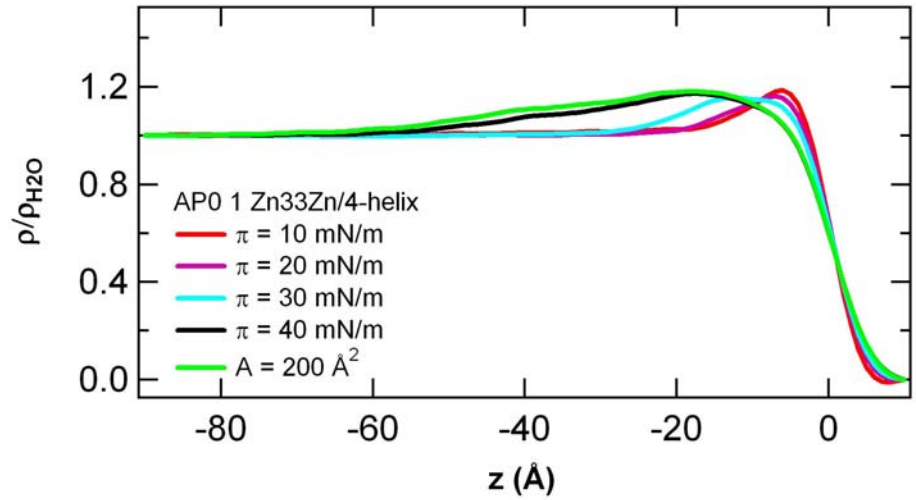

GIXD from apo-AP0

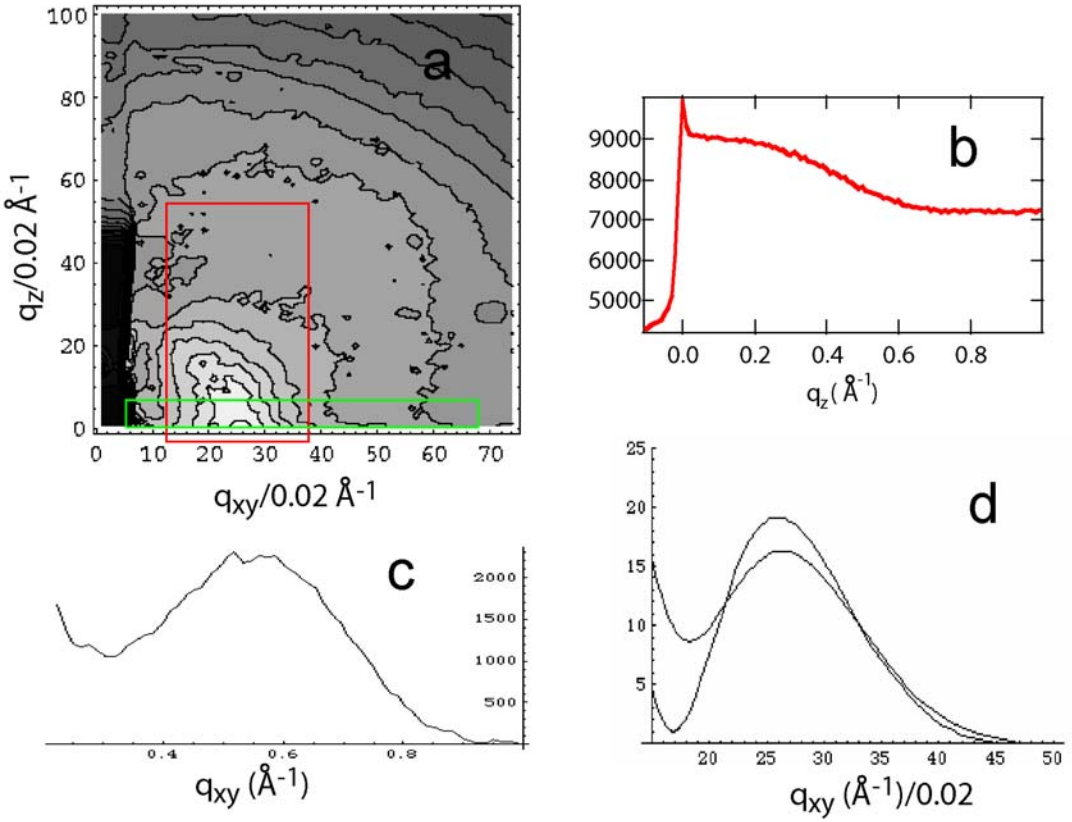

GIXD
Apo- vs. Holo-AP0 & Zn-3-3-Zn

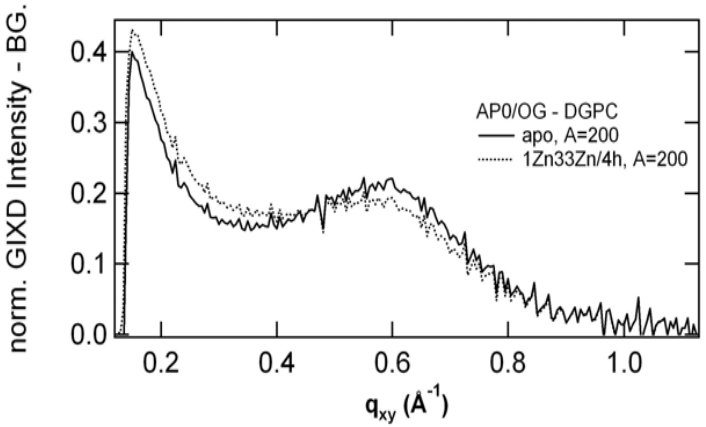

GIXD(q_{xy}-dependence) consistent with 4-helix bundles (4-cylinder model, 8Å diameter cylinders @ 10Å inter-helix spacing), allowing for Δ q_{xy}-resolution and GIXD(q_z-dependence) consistent with coiled-coil with pitch of major helix of ~100Å and pitch angle of ~17^0

Reflectivity from apo-AP2 & holo-AP2 for 2 Zn-3-3-Zn/4-helix bundle

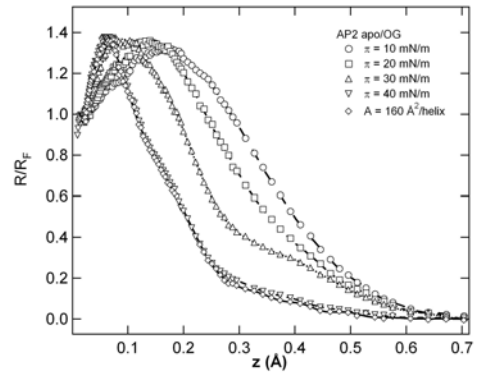

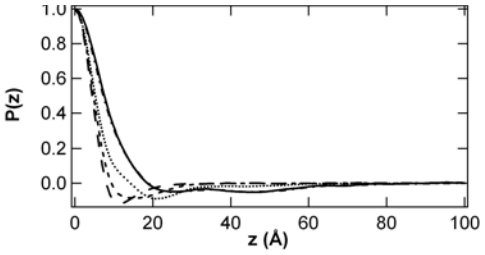

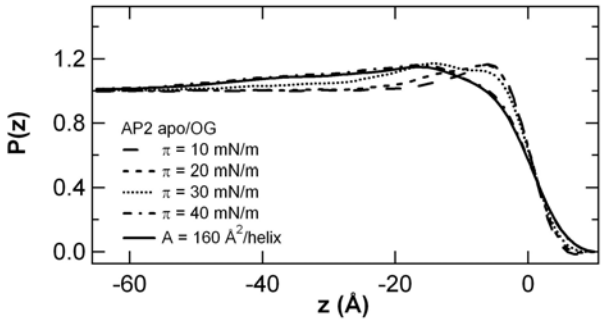

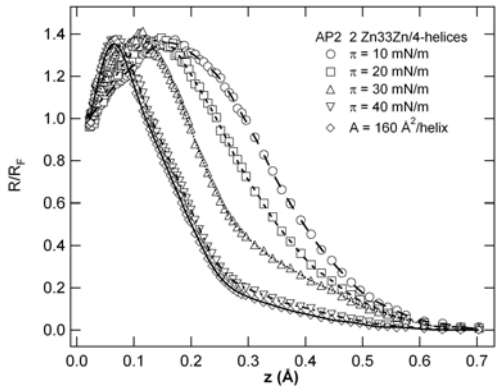

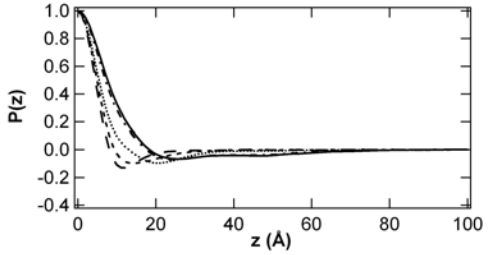

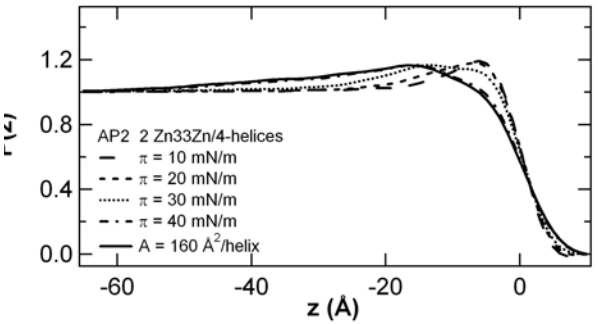

apo-AP2 *vs.* apo-AP3

Δ = 14-residues in hydrophilic domain

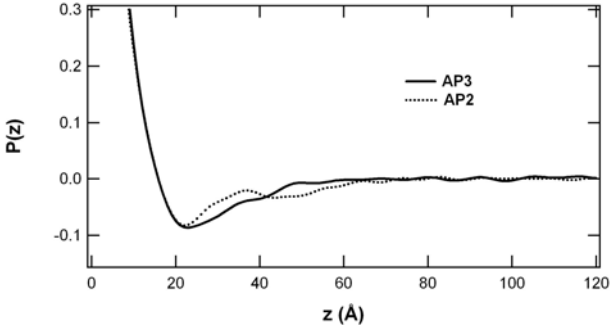

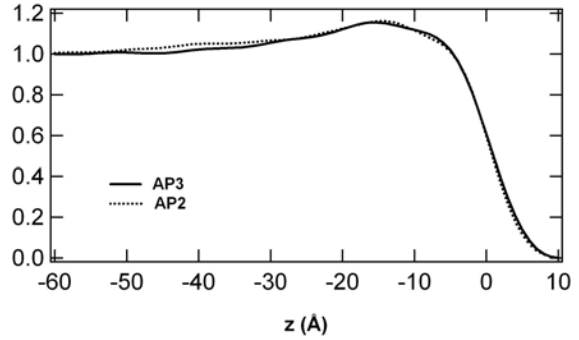

GIXD apo-AP2

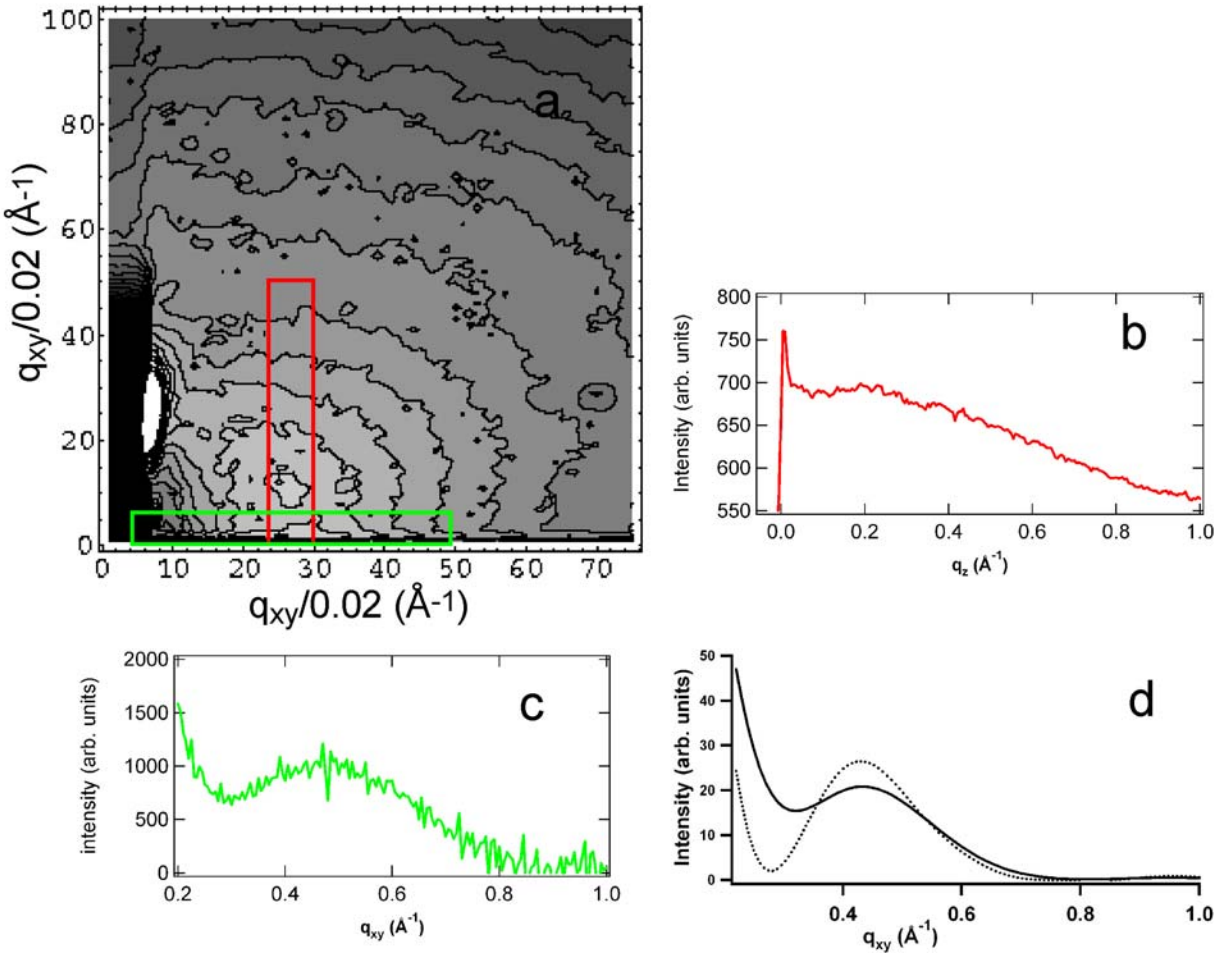

GIXD(q_{xy}-dependence) consistent with 4-helix bundles;
(4-cylinder model, 10Å diameter cylinders @ 12Å inter-helix spacing)

GIXD(q_z-dependence) consistent with coiled-coil
with pitch of major helix of ~125Å and pitch angle of ~14^0

Results-to-Date Summary

- AP0, AP2 & AP3 peptides vectorially orient in Langmuir monolayers at the air/water interface as stable 4-helix bundles, with the bundle axis normal to the plane of the interface at higher surface pressures
- AP2 & AP3 bind biological redox cofactors (via axial histidyl ligation) at selected positions within both hydrophilic & hydrophobic domains
- AP2 & AP3 are able to bind several different redox cofactors, e.g., metalloporphyrins & metal-substituted chlorophylls, thereby providing electron-donor pairs with selected separations along bundle axis
- AP0, AP2 & AP3 can also bind non-biological cofactors (via axial histidyl ligation) at selected positions within both hydrophilic & hydrophobic domains thereby providing designed electron-donor pairs within a single cofactor
- AP0-AP3 can orient with the electron transfer vector perpendicular to AND across the interface $\Rightarrow$ potential materials applications

Intra-Bundle Structure

MD simulation vs. neutron reflectivity of

amphiphilic di-helical peptide BBC16 with selectively ^{2}H-labeled leucine residues

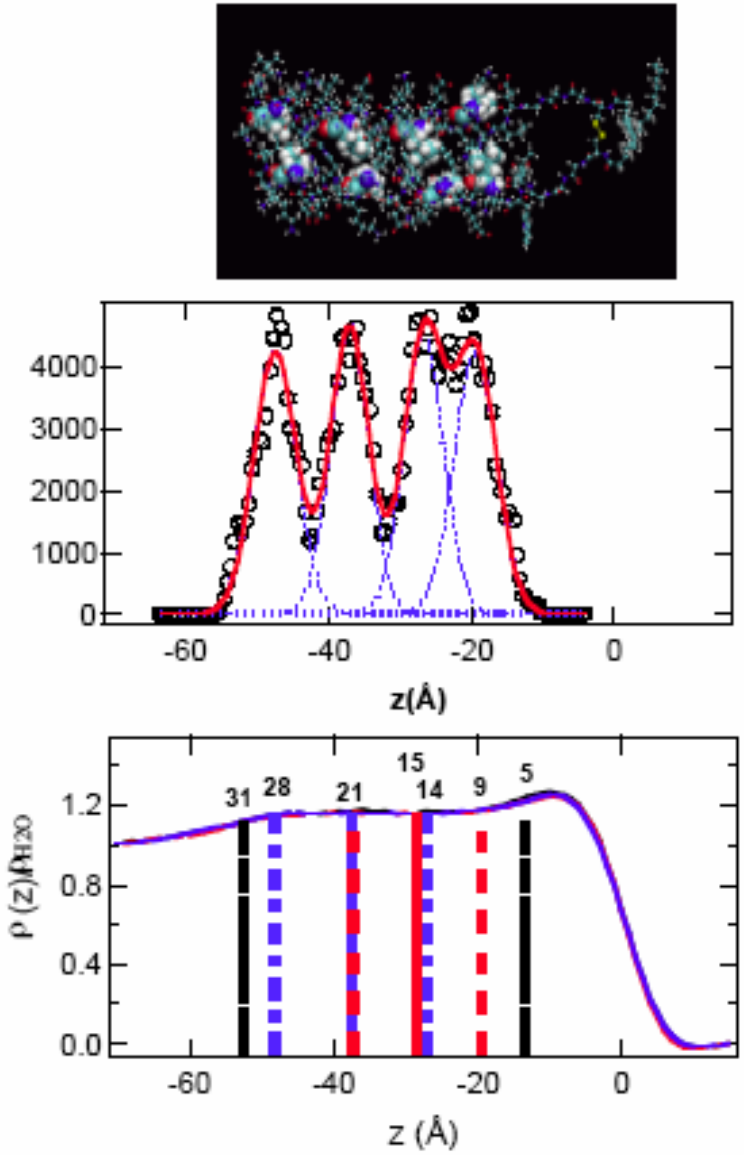

Molecular Dynamics (MD) simulation of an ensemble of sixteen alkylated di-helical peptides, vectorially-oriented in a Langmuir monolayer at the air-water interface upon compression; the helix orientation is perpendicular to the monolayer plane. The instantaneous configuration of one di-helix within the equilibrated ensemble is shown to scale in the top frame. Leucine residues at the 09, 14, 21, and 28 positions in the sequence shown in the CPK representation. The air-water interface is located at z=0Å with the aqueous sub-phase to the left at negative z-values. The time-averaged distribution of these four leucine residues within the ensemble profile structure is shown in the middle frame as the open circles; the non-linear least-squares best fit to this distribution (red), and modeling the distribution of each leucine residue as a Gaussian function (blue dotted). The mean positions of these four leucine residues agree very well (but not exactly) with those determined by neutron reflectivity, employing selective deuteration of each of these four leucine residues, summarized in the bottom frame. The experimentally determined positions of the residues are shown, determined to an accuracy of ±0.5Å, superimposed on the isomorphous electron density profiles for the fully-hydrogenated and the four selectively deuterated peptides.

Conclusions Re-Peptide Intra-Bundle Structure

- ^{2}H-labelled residues can be localized to within ±0.5Å within the monolayer profile structure via neutron reflectivity & solution of the phase problem, BUT absolute requirement for isomorphism between monolayers of the fully-hydrogenated peptide and selectively labelled peptides, which must be demonstrated, e.g., via X-ray reflectivity.

- MD simulations can provide agreement with experimental results of lower dimension, thereby providing a 3-D atomic level view. This will be key to understanding the effect of cofactor intercalation via specific binding at selected locations within the cores of the 4-helix bundle peptides.

WHY does it matter???

- X-ray crystal structures remain problematical (one to date!) and they're of questionable relevance

- NMR structures also remain problematical (also only one to date!) and they're of also questionable relevance

- NEED structure at the interface, namely
  both intermolecular & intramolecular!

- NEED structure at the interface, for both apo- and holo-forms, latter depending on nature & number of cofactors/4-helix bundle!

- Atomic resolution 3-D structure utilizing Molecular Dynamics simulation with experimental results as primary constraints

Collaborators

- **Ting Xu, Joseph Strzalka, Shixin Ye, Bohdana Discher, Erik Nordgren, Hongling Zou, Sophia Wu, Dror Noy, Chris Moser, Michael Therien & Les Dutton--**
  Departments of Chemistry and Biochemistry & Biophysics
  University of Pennsylvania

- **Sushil Satija, Chuck Majkrzak, Susan Krueger--**
  NG-7 & CNBT/NIST

- **Elaine DiMasi, Ben Ocko--X22B/NSLS/BNL**

- **Thomas Gog, Ivan Kuzmenko--CMC-Sector9/APS/ANL**

- **Funding--DOE (MS&E); NSF (MRSEC) re-APS/ANL; NIH (CNBT) re-NCNR/NIST**